Computers and Electronics in Agriculture 241 (2026) 111274

Contents lists available at ScienceDirect

Computers and Electronics in Agriculture

journal homepage: www.elsevier.com/locate/compag

Monitoring of rubber tree powdery mildew by combining spatial-spectral features and plant traits quantified from UAV hyperspectral imagery☆

Xiangzhe Cheng [a,b,c], Wenjiang Huang [a,b,c,*], Anting Guo [d,e,*], Zhiying Cai [f,g], Yingying Dong [a,b,c], Bohai Hu [a,b,c], Guiliang Chen [f,g], Haipeng Su [f,g], Lanlan Li [f,g]

[a] Key Laboratory of Remote Sensing and Digital Earth, Aerospace Information Research Institute, Chinese Academy of Sciences. Beijing 100101, China
[b] University of Chinese Academy of Sciences, Beijing 100049, China
[c] Sino-UK Pest and Disease Forecasting & Management Joint Laboratory
[d] School of Automation and Electrical Engineering, University of Science and Technology Beijing, Beijing 100083, China
[e] Key Laboratory of Knowledge Automation for Industrial Processes of Ministry of Education, Beijing 100083, China
[f] Yunnan Key Laboratory of Sustainable Utilization Research on Rubber Tree, Yunnan Institute of Tropical Crops, Jinhong 666100, China
[g] National and Local Joint Engineering Research Center of Breeding and Cultivation Technology of Rubber Tree, Yunnan Institute of Tropical Crops, Jinhong 666100, China

ARTICLE INFO

Keywords:
Remote sensing
Disease monitoring
UAV hyperspectral images
Rubber tree powdery mildew
Radiative transfer model
Pigments

ABSTRACT

Powdery mildew is a major disease affecting rubber tree yield. Rapid and accurate monitoring of this disease is crucial for plantation management. Previous studies have focused on spectral and spatial data for monitoring powdery mildew but have not adequately addressed the underlying physiological and biochemical alterations induced by the disease. Therefore, this study proposes a method combining spatial-spectral features and plant traits to monitor rubber tree powdery mildew. Unmanned Aerial Vehicles (UAVs) equipped with the ULTRIS X20P hyperspectral sensor (350–1000 nm) were used to capture hyperspectral imagery in two rubber plantations. Plant traits (PTs), including chlorophyll (Cab), carotenoids (Car), anthocyanins (Anth), leaf water content (Cw), and dry matter content (Cm), were inverted from UAV hyperspectral imagery using a radiative transfer model. Meanwhile, spectral and spatial information in the imagery were analyzed to extract vegetation indices (VIs), texture features (TFs), and color features (CFs) sensitive to the disease. Machine learning algorithms, including Partial Least Squares Regression (PLSR), Least Absolute Shrinkage and Selection Operator (LASSO), and Random Forest Regression (RF), were subsequently employed to create disease monitoring models based on these features. The results show that models based on VIs and TFs effectively monitor powdery mildew, with the inclusion of PTs significantly improving model performance. Models that integrate multiple features outperform those that depend on single features, especially the monitoring model integrating VIs, TFs, and PTs using the PLSR algorithm, which achieved an R^2 of 0.794 and an RMSE of 7.991. This study highlights the novelty of integrating spatial-spectral features with plant traits for monitoring rubber tree powdery mildew, offering a reference for precise disease monitoring through the use of UAV hyperspectral imagery.

1. Introduction

The rubber tree (*Hevea brasiliensis*) is an evergreen tree species native to tropical and subtropical regions, known for its production of natural rubber. It serves as a vital material in various industries, including industrial manufacturing, defense, and healthcare, and holds significant economic value (Van Beilen and Poirier, 2007). According to the Food and Agriculture Organization of the United Nations (FAO), the global export value of natural rubber was approximately USD 16.1 billion in 2022(FAO, 2024). However, pests and diseases in rubber trees are key factors limiting the high yield and quality of natural rubber. Among these, powdery mildew is one of the most prominent diseases, caused by the pathogen *Oidium heveae Steinmann*. It primarily infects buds, tender stems, leaves, and inflorescences of rubber trees. Such infections cause secondary leaf drop, delay the onset of tapping, reduce latex yield, induce seed loss, weaken growth, and may even result in the death of

☆ This article is part of a special issue entitled: 'Agricultural Cybernetics' published in Computers and Electronics in Agriculture.

* Corresponding authors.
E-mail addresses: huangwj@aircas.ac.cn (W. Huang), guoat@ustb.ac.cn (A. Guo).

https://doi.org/10.1016/j.compag.2025.111274
Received 22 January 2025; Received in revised form 28 September 2025; Accepted 27 November 2025
0168-1699/© 2025 The Author(s). Published by Elsevier B.V. This is an open access article under the CC BY-NC-ND license (http://creativecommons.org/licenses/by-nc-nd/4.0/).

new shoots (Limkaisang et al., 2005). Currently, the control of rubber tree powdery mildew relies on setting up monitoring points, regularly collecting leaf samples during the peak disease period for diagnosis, and using weather forecasts to guide pesticide spraying for chemical control. While relatively ideal control outcomes can be achieved in localized areas, effective control still requires considerable human and material resources in actual plantation operations, such as manual sprayers, with one worker treating about 50 mu per day, which constrains the scientific and precise management of rubber plantations. Therefore, developing rapid and accurate monitoring techniques tailored for plantation-scale management is essential to enhance disease control efficiency and improve the precision of rubber plantation management.

Remote sensing is a technology that relies on sensors for non-contact, long-distance target detection, providing an effective means for quickly obtaining spatiotemporal continuous information over large areas (Bravo et al., 2003). It has been extensively used in crop disease monitoring research (Zhang et al., 2012b). The theoretical basis of remote sensing technology for crop disease monitoring is that different diseases cause distinct symptoms and crop damage, resulting in varying spectral responses. Therefore, by analyzing crop spectral features, disease occurrence and severity can be assessed (Moshou et al., 2005). Recent advancements in Unmanned Aerial Vehicle (UAV) remote sensing technology have further expanded its application at the plantation level. UAVs offer high temporal and spatial resolution and can carry diverse sensors for real-time imaging, enabling timely crop disease monitoring even when cloud or rain limits optical satellite imagery acquisition (Ecke et al., 2022). Scholars have utilized UAVs to monitor various crop diseases and achieved significant research results. Bhandari et al. (2020) obtained spatial images of wheat fields using a Red-Green-Blue (RGB) sensor mounted on a UAV and monitored the severity of wheat leaf rust by calculating three vegetation indices, the Normalized Difference Index (NDI), the Green Index (GI), and the Green Leaf Index (GLI). Su et al. (2018) created a monitoring model for wheat stripe rust utilizing UAV-based multispectral images and a Bayesian-optimized Random Forest technique, with an accuracy of 89.3 %.

In UAV-mounted sensors, hyperspectral sensors provide considerable advantages for crop disease monitoring due to their superior spatial resolution and rich spectral information, enabling continuous capture of spectral and image data (Calderón et al., 2013). Researchers have mostly employed spectral features that indicate physiological and biochemical changes, such as pigments and moisture content, to monitor crop diseases. Common methods include vegetation indices (Ashourloo et al., 2014), fractional-order differentiation (Huang et al., 2019), optimal wavelength selection from original spectra (Deng et al., 2020), and continuous wavelet transform (Zhang et al., 2012a). Among them, vegetation indices (VIs), which improve spectral differences through band combinations and transformations, have been widely applied in crop disease research as a simple and efficient method for describing spectral changes (Zhang et al., 2019). Abdulridha et al. (2020) derived 29 VIs from UAV hyperspectral imagery of squash fields, finding that four indices, Cl_{green}, $ND_{750/705}$, GNDVI, and SR_{850}, were effective in identifying different stages of squash powdery mildew. When crops are infected, they undergo internal physiological and biochemical changes as well as external alterations in traits such as leaf color, leaf texture, and overall morphology. Thus, incorporating spatial features like texture and color can enhance crop disease detection accuracy (Zheng et al., 2019). Guo et al. (2020) developed disease monitoring models for wheat yellow rust based on VIs and texture features (TFs) obtained from UAV hyperspectral imagery, finding that models combining VIs and TFs yielded the best performance across all infection stages. In recent years, several studies have also employed spectral bands, VIs, TFs, and color features (CFs) extracted from UAV multispectral or hyperspectral imagery to monitor and assess the occurrence and severity of powdery mildew in rubber trees (Zeng et al., 2023). Although these features have been proven effective for estimating the severity of various crop diseases, they still primarily rely on canopy-scale spectral reflectance and spatial appearance, lacking the capacity to directly quantify the internal physiological and biochemical changes induced by disease stress.

Plant traits (PTs), such as pigment levels, dry matter, moisture content, and vegetation structure, are strongly linked to crop health and their response to disease stress (Hornero et al., 2020). Compared to spatial-spectral features, PTs more directly capture the physiological and biochemical changes in crops following disease infection, thus gaining more attention in crop disease monitoring (Zhao et al., 2016; Martins et al., 2017). Wu et al. (2023) inverted several PTs, including canopy chlorophyll content, leaf area index, tree height, and canopy area, from UAV hyperspectral imagery of jujube fruits during fruit expansion, and developed a health assessment model. Presently, PTs are mostly acquired by two approaches: statistical techniques and radiative transfer models (RTM). The former correlates remote sensing features (e.g., spectral bands and vegetation indices) with ground measurements via conventional statistical modeling and machine learning methodologies (Jiang et al., 2021). The latter involves the physical processes of vegetation canopy and solar radiation interaction, using RTM and spectral data to invert crop PTs (Camino et al., 2021; Verrelst et al., 2015). These studies demonstrate the advantages of PTs in crop disease monitoring. However, studies on PTs-based monitoring of rubber tree powdery mildew remain restricted, especially regarding the use of RTM to invert PTs. Hence, the potential of PTs for monitoring rubber tree powdery mildew warrants further exploration.

In response to the limited investigations on PTs inversion in rubber trees using RTM and the insufficient studies combining PTs for rubber tree powdery mildew monitoring, this study explicitly aims to address this gap by proposing an effective method for monitoring rubber tree powdery mildew through the integration of spatial-spectral features and plant traits quantified from UAV hyperspectral imagery. The key goals of this study are therefore twofold: (1) to comprehensively evaluate the performance of VIs, TFs, and CFs extracted from UAV hyperspectral imagery, combined with PTs inverted from RTM, in monitoring rubber tree powdery mildew; (2) to construct a novel monitoring model for rubber tree powdery mildew that synergistically leverages spatial-spectral features and plant traits. This study advances current disease-monitoring methodologies and provides technical support for the precise monitoring and management of rubber tree powdery mildew in plantations.

2. Materials and methods

2.1. Overview of the study area

The study was conducted in the Rubber Tree Research Area of the Yunnan Institute of Tropical Crops, located in the Xishuangbanna Dai Autonomous Prefecture, Yunnan Province, southwestern China. The area is situated at 22 °2 ′N, 100 °52 ′E, with an elevation of 852.2 m. Characterized by a warm and humid climate throughout the year, the region experiences average annual temperatures ranging from 19.6°C to 25.6°C, with annual rainfall varying between 627.5 mm and 1196.6 mm. The experiment took place from March 8 to March 11, 2024, at two different locations: Ganlanba Farm (21 °49 ′59 ″N, 100 °56 ′21 ″E) and Dongfeng Farm (21 °39 ′43 ″N, 100 °44 ′50 ″E) in Jinghong City (Fig. 1). The rubber trees in the study area are of the Yunyan 77–2 cultivar, planted in 2011, with an average age of 13 years at the time of the study. They were planted with a row spacing of approximately 10 m and a plant spacing of about 2 m, and had an average height of about 18 to 20 m and a canopy width of 3 to 4 m. During this period, the phenology of rubber trees ranged from bronze to pale-green, making it an important time to monitor and prevent powdery mildew. All trees were under standard plantation management, with no visible signs of abiotic stress other than powdery mildew symptoms.

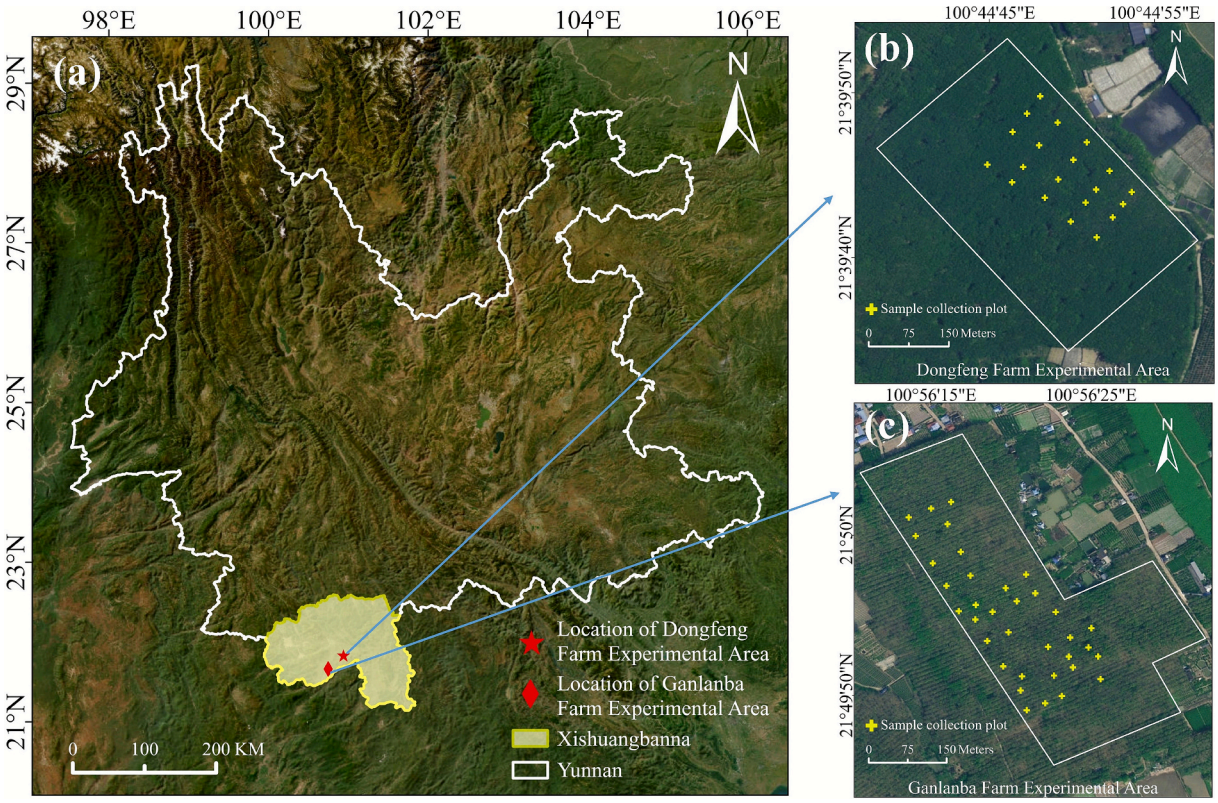


Fig. 1. Location of the study area and distribution of sampling plots. (a) Yunnan Province, (b) Dongfeng Farm, (c) Ganlanba Farm.

2.2. Data acquisition and processing

2.2.1. Field data acquisition

In the experimental area, 55 sampling plots were evenly distributed, each consisting of 2 × 2 rubber trees (4 trees per plot). The geographical coordinates of the center of each sampling plot were obtained using a Real-time kinematic (RTK) measurement instrument. The severity of powdery mildew on rubber plants at each sampling plot was described using a disease index (DI). During sampling, a telescopic pruner was used to cut a suitable number of leafy clusters toward the top of the rubber tree canopy from the four cardinal directions (east, south, west, and north), approaching the crown region directly observable by the UAV. Given that rubber tree leaves are trifoliate, 50 middle leaflets were then randomly selected from the collected clusters per plot for disease severity assessment. The assessment followed the technical guidelines for monitoring and reporting rubber tree powdery mildew established by China in 2015 (NY/T1089-2015) (Cheng et al., 2024a). Based on the leaf morphology and lesion size, the disease incidence was classified into five levels (0 %, 12.5 %, 25 %, 50 %, 75 %), with 0 % representing a healthy state, 12.5 % indicating disease severity 1, and 75 % representing disease severity 4, as shown in Fig. 2. The DI is calculated according to the following formula (Huang et al., 2007):

$$DI = \frac{\sum xf}{n\sum f} \times 100 \quad (1)$$

where f represents the total number of leaves with each disease severity, x denotes the disease severity level, and n is the maximum disease severity (in this study, n = 5).

Additionally, plant traits were measured at the same time as the leaf sample. The SPAD-502 (Konica Minolta, Tokyo, Japan) is a handheld chlorophyll meter that can measure chlorophyll content in crop leaves in real-time, accurately, and non-destructively (Richardson et al., 2002). During the measurement, six readings were taken per leaflet at three positions: the upper third, middle third, and lower third from the leaf tip. The average of these readings was calculated for each leaflet, and the average SPAD value across the 50 leaflets was taken as the SPAD value of the corresponding plot. Finally, the unitless SPAD value was translated into chlorophyll content (μg/cm^2) using the following equation (Haboudane et al., 2002):

$$\mathrm{CHL} = 9.1411e^{0.0318\times SPAD} \quad (2)$$

where SPAD represents the SPAD value, and CHL denotes the chlorophyll content (μg/cm^2).



Fig. 2. Examples of powdery mildew at different infection stages: (a-e) Healthy (0%), Severity 1 (12.5%), Severity 2 (25%), Severity 3 (50%), and Severity 4 (75%).

2.2.2. UAV hyperspectral image acquisition

This study used a DJI M300 RTK quadcopter to acquire hyperspectral data (Fig. 3). The drone is capable of carrying a maximum payload of 9 kg and has a continuous flight duration of 55 min. It was equipped with a ULTRIS X20 Plus hyperspectral camera, which utilizes a 20 MP ultra-high-definition CMOS sensor as its core component. The camera uses frame-based imaging to rapidly capture hyperspectral images, covering a wavelength range from 350 to 1000 nm, with a 4 nm spectral resolution and 164 channels. Data collection at the Ganlanba and Dongfeng Farm experimental areas took place on March 10 and March 11, 2024, from 11:00 to 13:00, respectively, under clear skies with no clouds. The drone operated at an altitude of 150 m and a flight speed of 6 m/s, maintaining 80 % forward overlap and 70 % side overlap. Prior to each flight, radiometric calibration was conducted using both a white reference panel and a dark reference panel to ensure accurate reflectance retrieval. Due to battery limitations, data acquisition was completed in two flights at each experimental area, with identical flight parameters. The hyperspectral images obtained exhibited a spatial resolution of 4.5 cm/pixel.

2.2.3. UAV hyperspectral image processing

After acquiring the hyperspectral images, data preprocessing is required, including image fusion, stitching, and reflectance extraction. In this study, the Cubert-Pilot software (Cubert, Baden-Württemberg, Germany) was employed to merge each hyperspectral image with its corresponding panchromatic image acquired concurrently. The Agisoft Metashape Professional 1.7.6 software (Agisoft LLC, St. Petersburg, Russia) was then employed to stitch the hyperspectral images using the panchromatic images' point cloud data. Finally, radiometric calibration was applied based on the pre-flight dark and white reference measurements, where the dark panel was applied for dark current correction and the white panel served as a reflectance standard, enabling the conversion of digital number (DN) values into surface reflectance.

2.3. Extraction and analysis of features

2.3.1. Vegetation indices extraction

VIs, which combine sensitive spectral bands and spectral response anomalies, emphasize disease-specific spectral characteristics and have been widely applied in crop disease monitoring studies. Based on previous research, this study selected 39 VIs from relevant literature for monitoring rubber tree powdery mildew, which are related to pigments, structure, physiology, and water content. Their definitions, descriptions, and references are provided in Table S2. Examples of the extracted features are shown in Fig. 4.

The above four categories of VIs may not all contribute to rubber tree powdery mildew. By minimizing redundancy and selecting the most relevant features, the model's accuracy can be enhanced. Thus, the study employed the RReliefF (Regressional ReliefF) method to calculate feature weights and retain the most important ones, as this algorithm effectively evaluates the conditional dependencies between features and continuous target variables, making it particularly suitable for efficiently ranking features in regression-based modeling tasks.

RReliefF is an extension of the widely used feature selection algorithm ReliefF, specifically designed for regression tasks (Robnik-Šikonja and Kononenko, 2003). The core idea behind the ReliefF algorithm is to calculate feature weights by estimating their ability to distinguish similar samples. In classification tasks, ReliefF randomly selects a sample R from the sample set D, finds k near Hits (H) and k near Misses (M), and updates the weights based on the feature values of R, M, and H. However, because predicted values are continuous and categories are difficult to discern in regression tasks, RReliefF represents differences in predicted values with probabilities and calculates feature weights based on the distance between sample feature values and target values. The feature weight is determined using the following formula (Robnik-Šikonja and Kononenko, 2003):

$$W[A] := N_{d_C \& d_A}[A]/N_{d_C} - (N_{d_A}[A] - N_{d_C \& d_A}[A])/(m - N_{d_C}) \quad (3)$$

where N_{d_C} represents the total sum of target distances between all samples, $N_{d_A}[A]$ represents the cumulative difference of attribute values on feature A, and $N_{d_C \& d_A}[A]$ represents the cumulative joint difference between the target and feature A. m represents the number of samples.

2.3.2. Texture and color feature extraction

Texture is a visual characteristic that represents homogeneous phenomena in an image, containing important information about the surface structure and arrangement of objects. The extraction typically relies



Fig. 3. Field data collection, UAV equipment, and flight activities. (a) UAV used for hyperspectral data acquisition; (b) Original UAV-captured hyperspectral imagery; (c) UAV flight operations; (d) Leaf sampling classification and RTK positioning; (e) On-site leaf clipping process.

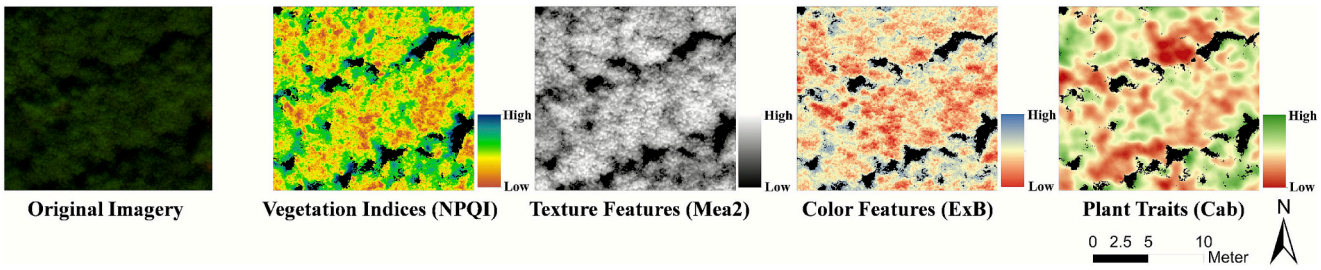


Fig. 4. Examples of the extracted features.

on various techniques, including statistical, geometric, model-based, structural, and signal-processing methods. Among these, the Gray-Level Co-occurrence Matrix (GLCM) is a commonly used method in crop disease monitoring research, capturing texture information by statistically analyzing the grayscale relationships between two pixels separated by a specific distance (Haralick et al., 1973). This study chose eight commonly used TFs: Contrast (Con), Correlation (Cor), Dissimilarity (Dis), Entropy (Ent), Homogeneity (Hom), Mean (Mea), Second Moment (Sec), and Variance (Var) (Baraldi and Panniggiani, 1995). Before extracting TFs, Principal Component Analysis (PCA) was used to decrease data redundancy and computational cost on hyperspectral images, as it effectively concentrates the most informative variance into fewer components, resulting in images with only the top three principal components (Guo et al., 2021). These three bands preserved the majority of the image's information, with a cumulative variance greater than 97 %. TFs were extracted using ENVI 5.3 software with 8 quantization levels, a pixel distance (d = 1), and a 3 × 3 sliding window, with texture values averaged across four directions (0°, 45°, 90°, and 135°), resulting in 24 TFs from the three bands.

CFs are global features that describe the surface properties of the objects corresponding to an image or image region. At the early stages of infection, radial silvery mycelium emerges on rubber tree leaves. As the disease progresses, the mycelium forms and produces spider-like, radial lesions before creating irregularly sized powdery mildew patches. In severe situations, the leaves get covered with powder, resulting in wrinkling, distortion, yellowing, and eventually falling of the leaves (Liyanage and Jacob, 1992). Therefore, CFs have potential value for identifying powdery mildew severity. This study used hyperspectral images at 694, 542, and 482 nm to synthesize RGB images and extract 12 CFs (Zhang et al., 2022). Definitions, descriptions, and references are provided in Table S3. Examples of the extracted features are shown in Fig. 4.

2.3.3. Plant traits extracted based on hybrid model

This study combined the PROSAIL model with the Gaussian Process Regression (GPR) algorithm in a hybrid model to retrieve PTs. First, the PROSAIL model was used to generate simulated spectral data and their corresponding PTs. Based on this, the GPR algorithm was applied to build a relationship model between the simulated spectra and the PTs, which was further applied to real spectral data for parameter inversion (Tagliabue et al., 2022).

PROSAIL is a coupled model of the leaf optical characteristics model PROSPECT and the canopy radiative transfer model SAIL, which has been widely used in PTs inversion and spectral simulation (Jacquemoud et al., 2009). Several versions of the model have been developed for different research needs. This study generated the simulated dataset using the PROSAIL-D (PROSPECT-D + 4SAIL) version in forward mode, with input parameters based on existing literature (Wang, 2014; Xu et al., 2022) and calibrated based on drone flight time and task settings. Table 1 shows specific parameters.

In this study, 10,000 simulated datasets were generated using the ARTMO tool (https://artmotoolbox.com) and divided into training and validation sets (7:3 ratio) for hybrid model construction (Verrelst et al., 2012). The GPR-based inversion model was developed using the MLRA module in ARTMO (Caicedo et al., 2014), and its performance was assessed using the coefficient of determination (R^2), root mean square error (RMSE), and mean absolute error (MAE). Due to the limited real data, only the Cab inversion performance was validated. Previous research has demonstrated this method's potential in crop disease detection (Poblete et al., 2020, 2021). The hybrid model was then applied to hyperspectral images for the accurate retrieval of PTs. Examples of the extracted features are shown in Fig. 4.

Table 1
Parameter settings of the PROSAIL model for generating the simulated dataset.

Model	Parameter	Description	Unit	Range
PROSPECT-D	N	Leaf structure	unitless	1–1.5
	C_{ab}	Leaf chlorophyll content	μg cm^{-2}	25–45
	C_{ar}	Leaf carotenoid content	μg cm^{-2}	2–20
	Anth	Leaf anthocyanin content	μg cm^{-2}	0–5
	C_{brown}	Brown pigment content	arbitrary units	0
	C_m	Dry matter content	g cm^{-2}	0.001–0.02
	C_w	Leaf water content	cm	0.01–0.2
4SAIL	LAI	Leaf area index	m^2 m^{-2}	2–5.5
	hspot	Hot spot effect	m m^{-1}	0.1–0.5
	angl	Average leaf angle	deg	30–80
	tts	Solar zenith angle	deg	25–70
	skyl	Diffuse/Direct radiation	unitless	0–100
	tto	Observer zenith angle	deg	0–80
	psoil	Soil brightness	unitless	0–1
	psi	Relative azimuth angle	deg	0–120

2.4. Severity estimation model construction and accuracy assessment

This study constructed a rubber tree powdery mildew monitoring model using the VIs, TFs, CFs, and their combinations with PTs (VIs + PTs, TFs + PTs, CFs + PTs, VIs + TFs, VIs + TFs + PTs) as feature variables, combined with Partial Least Squares Regression (PLSR), Least Absolute Shrinkage and Selection Operator (LASSO), and Random Forest Regression (RF) methods.

PLSR is a multivariate statistical analysis method that identifies the most relevant feature vector combinations in a high-dimensional space of independent and dependent variables, and projects them into a lower-dimensional space to establish a linear relationship between independent variables (X) and dependent variables (Y) (Wold et al., 2001). This method effectively addresses multicollinearity among variables and enhances model interpretability and robustness. The calculation formula is as follows:

$$Y = b_0 + b_1X_1 + b_2X_2 + \cdots + b_pX_p \quad (4)$$

where b_0 is the intercept, b_i is the regression coefficient, and p is the number of independent variables. In this study, the independent variables were the extracted VIs, TFs, CFs, and PTs, and the dependent variable was the DI value. LASSO is an improved linear regression method that introduces a regularization term to achieve feature selection and coefficient shrinkage, which effectively controls model complexity and mitigates overfitting risks, thereby optimizing predictive performance and interpretability (Tibshirani, 1996). RF regression is a powerful ensemble learning method that constructs multiple decision trees and combines random feature selection and bootstrapping to generate training samples, thereby improving the model's generalization ability and predictive accuracy (Breiman, 2001).

To better assess the accuracy and stability of the monitoring models, this study used Leave-One-Out Cross-Validation (LOOCV) for model training and validation, which is particularly suitable for small-sample scenarios as it minimizes partition-induced variability. In each LOOCV iteration, one sample served as the validation set, while the remaining samples were used for training. This process was repeated to ensure each sample was used for validation once. Model performance was evaluated by averaging the metrics over all iterations, ensuring efficient data use and preventing overfitting (Maimaitijiang et al., 2019). To further ensure the robustness of the models, all hyperparameters were optimized through grid search. The evaluation metrics for the model included R^2, RMSE, and relative root mean square error (RRMSE). Model development and analysis were performed on Windows 10, utilizing the scikit-learn machine learning library version 1.3.2 in Python (Anaconda 3, conda version 23.7.4).

3. Results

3.1. Assessment of the effectiveness of spatial-spectral features and plant traits in rubber tree powdery mildew monitoring

3.1.1. Spatial-spectral features

The spectral feature weights were calculated using the RReliefF method, with results shown in Fig. 5. A threshold of 0.04 was applied, resulting in the selection of seven VIs (OSAVI, PPR, PRI, RVSI, FCI, FRI1, and NPQI) with higher weights for further model development. While OSAVI, PPR, and PRI are associated with leaf pigment content, RVSI reflects leaf structure, and FCI, FRI, and NPQI are linked to leaf physiological responses.

The study selected spatial features sensitive to powdery mildew through correlation analysis, quantified using the correlation coefficient (|R|). Table 2 shows the correlation values and significance levels between spatial features and DI. Most spatial features exhibited strong correlations with DI (|R|: 0.3–0.85; $p < 0.01$), with TFs generally exhibiting higher correlations than CFs (e.g., ExG: $|R| = 0.4784$; Mea3: $|R| = 0.8546$). Selecting features sensitive to powdery mildew is essential to reduce data redundancy and processing complexity. However, simply choosing highly correlated features may overlook their high linear relationships. To address this, features with $|R| > 0.3$ and $p < 0.01$ were first selected. The subset was then optimized using Correlation-based Feature Selection (CFS), which heuristically balances minimizing inter-feature redundancy with maximizing correlation to the target variable. This approach ensures a representative yet low-redundancy feature set, which is critical for robust modeling with spatial-spectral data. Finally, 7 TFs (Cor1, Mea2, Dis2, Var3, Hom3, Ent3, Sec3) and 3 CFs (ExB, ExG, ExGR) were selected to construct the model.

3.1.2. Plant traits obtained from hybrid model inversion

This study utilized a hybrid model to invert five PTs: chlorophyll (Cab), carotenoids (Car), anthocyanins (Anth), leaf water content (Cw), and dry matter content (Cm). All five parameters showed high inversion accuracy, with R^2 values exceeding 0.9, as detailed in Table 3. Additionally, field data validation for Cab yielded an inversion accuracy of R^2 of 0.437 and RMSE of 2.763. (Fig. S1), further demonstrating the model's feasibility in practical applications.

Correlation analysis between the five inverted parameters and DI showed significant differences across varying disease severities ($p < 0.05$); thus, all were incorporated into the disease model (Table S4). Based on expert recommendations, DI was categorized into four levels: healthy (DI ≤ 8 %), mild (8 % < DI ≤ 20 %), moderate (20 % < DI ≤ 50 %), and severe (DI > 50 %). The trends of the five parameters with disease severity are shown in Fig. 6, with Cab, Car, Cw, and Cm decreasing, while Anth increases as the disease progresses.

3.2. Performance evaluation of rubber tree powdery mildew monitoring models based on different features

Table 4 compares the DI estimation accuracy of rubber tree powdery mildew monitoring models constructed using different feature combinations and regression algorithms. When the three highly correlated CFs (ExB, ExG, ExGR) were used as inputs, the models built with PLSR, LASSO, and RF had R^2 values of 0.180, 0.348, and 0.238, respectively, indicating weak explanatory power for disease variation and limited

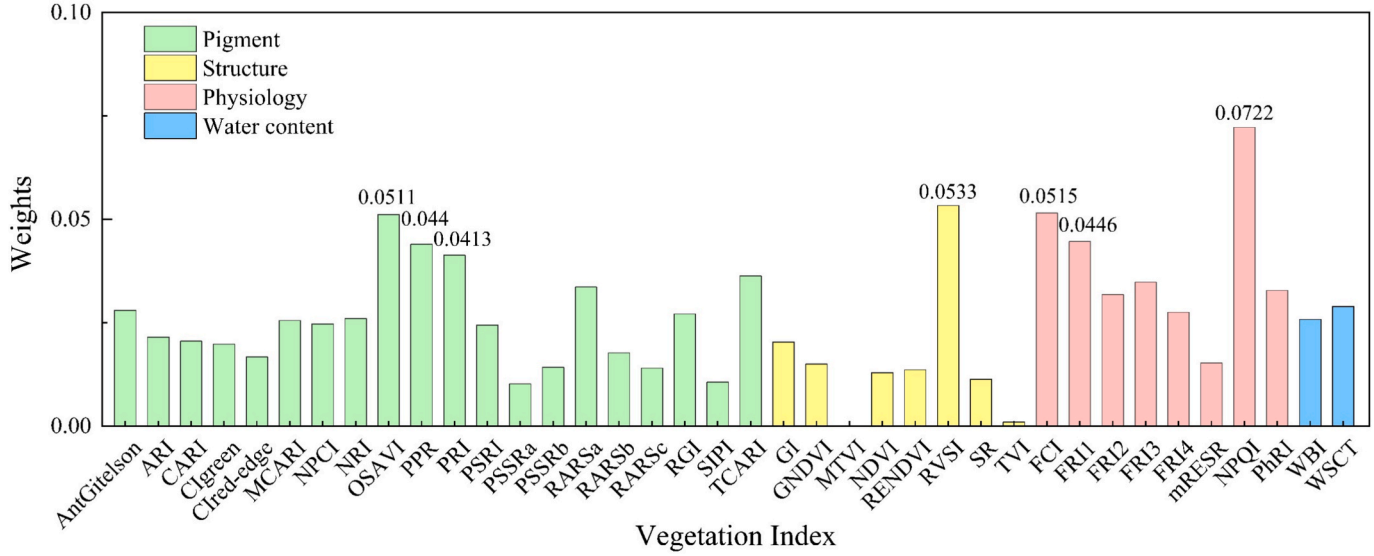


Fig. 5. The weights of VIs obtained by RReliefF.

Table 2
Correlation between spatial features and disease index.

Texture Parameter					
Feature	Coefficient ofCorrelation (R)	Feature	Coefficient ofCorrelation (R)	Feature	Coefficient ofCorrelation (R)
Mea1	−0.2185*	Mea2	0.5678**	Mea3	0.8546**
Var1	0.1243*	Var2	0.2247*	Var3	−0.8172**
Hom1	−0.2595*	Hom2	−0.3357**	Hom3	0.8213**
Con1	0.2595*	Con2	0.4263**	Con3	−0.8125**
Dis1	0.2595*	Dis2	0.4027**	Dis3	−0.8207**
Ent1	0.1726*	Ent2	−0.0058	Ent3	−0.8199**
Sec1	−0.1608*	Sec2	0.0400	Sec3	0.8133**
Cor1	−0.3532**	Cor2	−0.7311**	Cor3	0.7947**
Color Parameter					
Feature	**Coefficient of Correlation (R)**	**Feature**	**Coefficient of Correlation (R)**	**Feature**	**Coefficient of Correlation (R)**
ExB	0.4383**	GLA	0.1030*	RGBVI	0.1887*
ExG	−0.4784**	IKAW	0.1951*	VARI	−0.0138
ExGR	−0.3807**	MGRVI	−0.0036	VEG	0.1502*
ExR	−0.1744*	NGRDI	−0.0015	WI	−0.0257

Note: * and ** represent significance at $p < 0.05$ and high significance at $p < 0.01$, respectively.

Table 3
Accuracy metrics (R^2, RMSE, and MAE) of the hybrid model for retrieving PTs.

PTs	C_{ab}	C_{ar}	Anth	C_w	C_m
R^2	0.90	0.91	0.90	0.92	0.96
RMSE	1.9344	1.6404	0.0182	0.0012	0.001
MAE	1.4879	0.3470	0.0135	0.0004	0.0007

monitoring effectiveness. Using VIs as inputs, DI estimation accuracy significantly improved, with R^2 values exceeding 0.6, demonstrating the potential of spectral features for disease severity characterization. Using TFs as inputs yielded encouraging results, with R^2 values surpassing 0.65, and the PLSR model achieving 0.729, outperforming models with CFs and VIs as inputs, highlighting the importance of spatial features in capturing disease effects on leaf morphology.

Furthermore, models incorporating multiple features outperformed those with single ones. The VIs + TFs model, which combines spatial and spectral data, increased R^2 to 0.743 compared to models using VIs or TFs alone. The inclusion of PTs noticeably improves model performance. The inclusion of PTs led to a noticeable improvement in model performance, with the R^2 of CFs + PTs, VIs + PTs, and TFs + PTs combinations increasing by more than 0.02 compared to models using only CFs, VIs, or TFs. The model combining VIs, TFs, and PTs demonstrated the highest performance, with R^2 values of 0.794, 0.741, and 0.737 for PLSR, LASSO, and RF, respectively, outperforming the VIs + TFs model by 0.051, 0.014, and 0.023.

These results suggest that models integrating spatial-spectral features and plant traits can achieve superior performance compared to those without PTs, indicating the potential contribution of PTs in disease monitoring. Among all models, the VIs + TFs + PTs combination with PLSR yielded the best performance, achieving an R^2 of 0.794, RMSE of 7.991, and RRMSE of 0.284 (Fig. 7). This improvement likely results

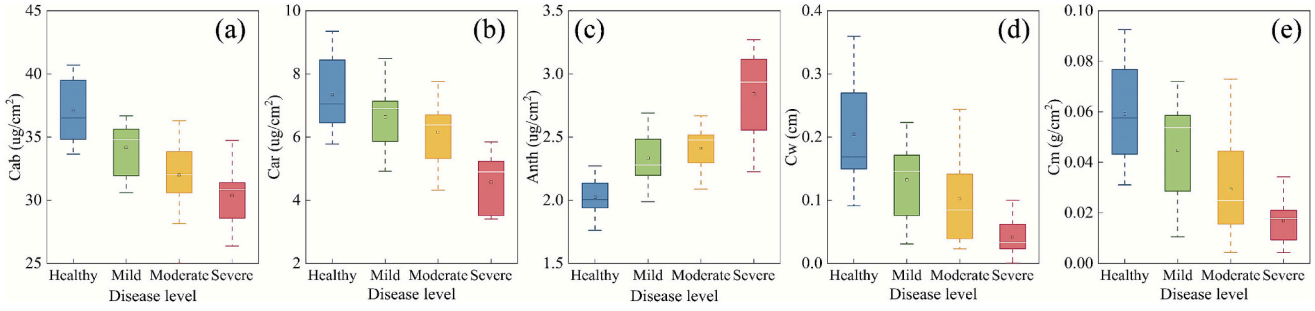


Fig. 6. Variations in inverted PTs across different disease severity levels. Panels (a–e) represent Cab, Car, Anth, Cw, and Cm, respectively.

Table 4
Accuracy of powdery mildew monitoring models based on different feature combinations and algorithms.

Input features	PLSR			LASSO			RF		
	R^2	RMSE	RRMSE	R^2	RMSE	RRMSE	R^2	RMSE	RRMSE
CFs	0.180	15.94	0.57	0.348	14.22	0.51	0.238	15.36	0.55
CFs + PTs	0.367	14.01	0.50	0.369	13.98	0.50	0.289	14.84	0.53
VIs	0.653	10.36	0.37	0.666	10.17	0.36	0.609	11.01	0.39
VIs + PTs	0.703	9.60	0.34	0.694	9.73	0.35	0.644	10.50	0.37
TFs	0.729	9.17	0.33	0.705	9.57	0.34	0.662	10.23	0.36
TFs + PTs	0.752	8.76	0.31	0.737	9.02	0.32	0.717	9.36	0.33
VIs + TFs	0.743	8.93	0.32	0.727	9.20	0.33	0.714	9.41	0.33
VIs + TFs + PTs	0.794	7.99	0.28	0.741	8.96	0.32	0.737	9.02	0.32

from the amplification and enhancement of spectral differences through band combinations, and sensitively captured morphological and structural changes induced by powdery mildew, while the inclusion of PTs provided a quicker response. The synergistic effect of these cross-dimensional features effectively compensated for the limitations of single features, further enhancing monitoring accuracy.

3.3. Mapping rubber tree powdery mildew severity in the study area

To assess the disease susceptibility of rubber trees within the study area, the study generated spatial distribution maps of rubber tree powdery mildew using the VIs + TFs + PTs model combined with PLSR, which showed the highest monitoring accuracy (Fig. 8). The results show that rubber trees in Ganlanba farm were severely infected, with the disease concentrated in the central and western areas, likely due to wind-driven spore spread and subsequent reinfection between plants. In contrast, rubber trees in Dongfeng farm exhibited lighter infections, mainly in the southern area, attributed to the preventive measure of spraying sulfur powder taken one week before the experiment. The observed disease occurrence and distribution in both study areas closely match the experimental results, further confirming the model's effectiveness.

4. Discussion

4.1. Features for monitoring rubber tree powdery mildew

Recently, UAV-based hyperspectral technology has been extensively employed in crop pest and disease monitoring. Hyperspectral data, covering a broad wavelength range, provides a wealth of spectral information, but it also causes substantial redundancy during spectral feature construction through band combinations and extracting texture features from spatial information. Therefore, feature selection is crucial for improving model accuracy. In this study, we used RReliefF to select sensitive VIs, followed by PCA, correlation analysis, and the CFS algorithm for TF selection. NPQI had the highest weight among the VIs selected by RReliefF, followed by RVSI. NPQI reflects chlorophyll degradation caused by disease-induced cellular damage, which reduces photosynthesis, and its role in crop disease monitoring is well established (Zarco-Tejada et al., 2018), and our findings further support this. RVSI captures disease-induced stress by detecting shifts in the red-edge inflection point related to chlorophyll concentration (Merton, 1998); as it primarily relies on bands near the red-edge endpoint (>730 nm), its variations may also indicate damage to leaf internal structures. Extracting TFs from the 164 original bands causes substantial data redundancy. To address this, PCA was used to convert the original image into three principal component images, retaining over 97 % of the variance. The selected TFs improved DI estimation accuracy to an R^2 of 0.729, demonstrating the method's efficiency and feasibility.

Compared to spatial-spectral features, PTs provide a more direct indication of the physiological and biochemical changes in crops caused by disease infection. A portable optical leaf-clip meter can precisely and non-destructively measure chlorophyll, anthocyanin, and other parameters in leaves. Previous studies using PTs from this meter have successfully enabled early detection of rubber tree powdery mildew at the leaf level (Cheng et al., 2024b). However, these types of equipment provide point-specific data, limiting their applicability for large-scale monitoring. Therefore, this study explored combining radiative transfer models with UAV hyperspectral imagery to estimate five PTs at the canopy scale. As powdery mildew infection progressed, Cab, Car, Cw, and Cm all decreased, while Anth increased. These changes are closely linked to the physiological processes of the leaf. Powdery mildew damages the photosynthetic structure of the leaf, inhibiting photosynthesis and causing chlorosis, necrosis, and pigment degradation (Oerke et al., 2016). The reduction in Cw and Cm further reflects the disease's impact on the internal and surface structures of the leaf, leading to stomatal dysfunction and increased water evaporation (Torriani et al., 2015). The increase in Anth is closely related to enhanced antioxidant activity, which may be a defense response to mitigate oxidative damage caused by powdery mildew infection (Alasalvar et al., 2001).

4.2. Rubber tree powdery mildew monitoring models based on different features

This study explored the application of VIs, TFs, CFs, and their combinations with PTs to construct a rubber tree powdery mildew

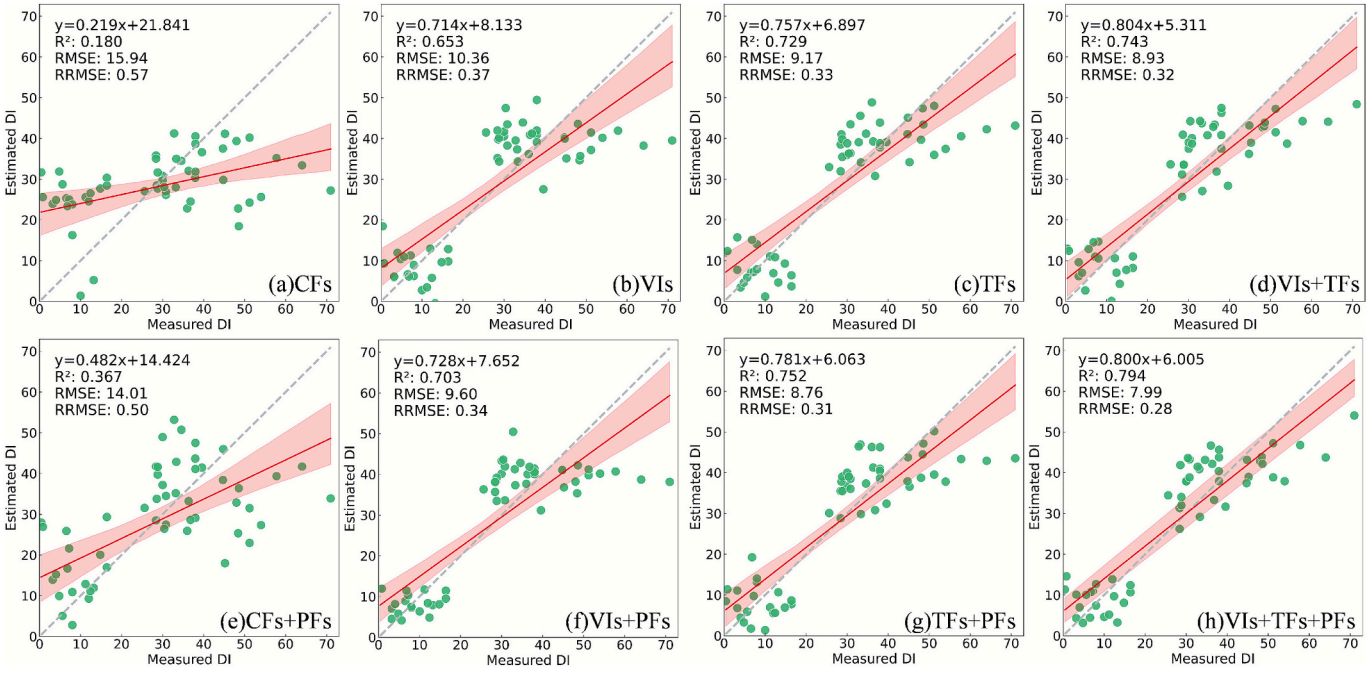


Fig. 7. Scatter plots of measured vs. estimated DI for models based on the PLSR algorithm using (a-h) CFs, VIs, TFs, VIs + TFs, CFs + PTs, VIs + PTs, TFs + PTs, and VIs + TFs + PTs. The red line shows the fitted regression with its 95 % confidence interval.

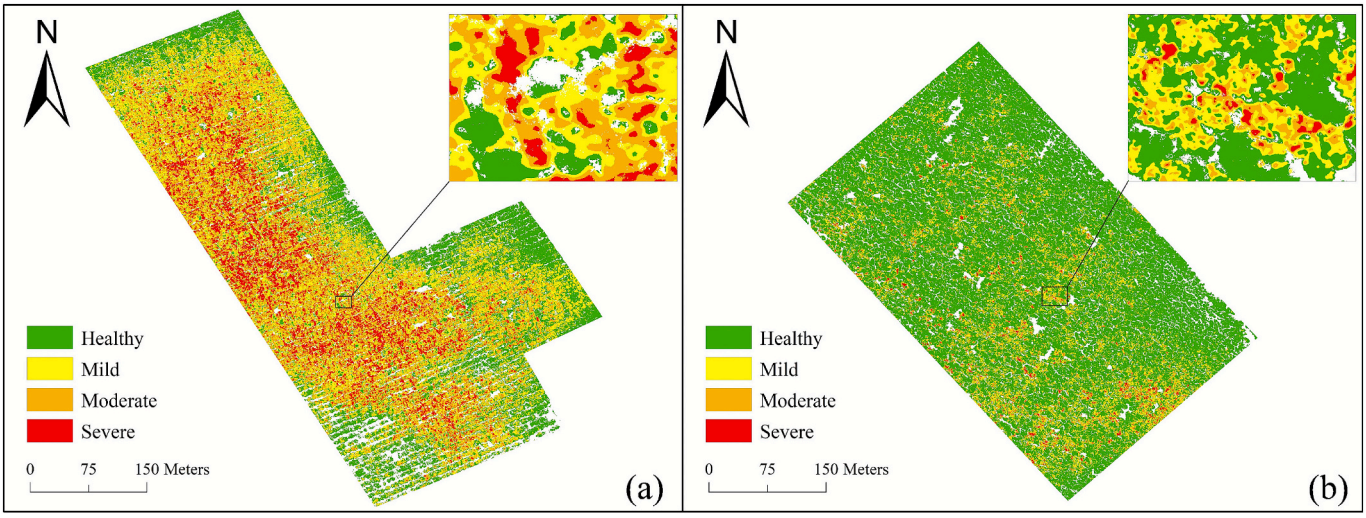


Fig. 8. Spatial distribution of rubber tree powdery mildew according to the best-performing model: (a) Ganlanba Farm, (b) Dongfeng Farm.

monitoring model. While VIs are widely employed in crop disease monitoring, their performance in this study was limited, likely due to their reliance on only a few bands that fail to provide detailed disease information. Additionally, the VIs used here are general indices, rather than those specifically developed for rubber tree powdery mildew. Future studies should aim at identifying rubber-tree-specific spectral bands most responsive to powdery mildew infection. Texture features, which capture subtle spatial structural changes in crops under disease stress, are often integrated with spectral data to overcome the limitations of spectral features in complex environments (Zhang et al., 2021). In this study, combining VIs and TFs improved model accuracy, with the PLSR-based model achieving an R^2 of 0.743, an increase of 0.090 and 0.014 over models using only VIs or TFs, respectively. This demonstrates that combining spectral and spatial features enhances the model's ability to capture both physiological and morphological changes, improving its performance. However, introducing CFs resulted in poor performance, with a maximum R^2 of 0.368. This may be attributed to uneven illumination as well as variations in canopy structure and shadowing in large rubber plantations, all of which reduce the stability of color feature extraction. While RGB drone systems are sensitive to lighting conditions, they remain cost-effective and portable, making them suitable for large-scale monitoring. Future research should explore more effective ways to integrate color features with other data to improve disease monitoring accuracy and stability.

In addition, performance differences among the three algorithms were observed when using the same feature combinations. Overall, except for models based on VIs and CFs + PTs, PLSR achieved higher R^2 values than LASSO and RF. This advantage may be attributed to the strength of PLSR in handling high-dimensional and multicollinear features, as it projects the original variables onto a lower-dimensional latent space that can more effectively capture key information related to disease severity. By contrast, LASSO benefits from strong variable selection and regularization capabilities to filter redundant features, but its performance can be limited when nonlinearity or interaction effects exist. Although RF has good capacity for nonlinear modeling and robustness to outliers, in this study, when the input feature information was insufficient or noisy (such as the unstable CFs), the random feature selection mechanism of RF might not fully utilize useful information, which affected the model's stability and generalizability. These findings highlight the importance of model selection in disease monitoring tasks, and also point to the potential of exploring more advanced approaches in the future.

Previous studies have relied solely on spatial-spectral features for powdery mildew detection, whereas this research emphasizes the combination of spatial-spectral features and PTs, with the inclusion of PTs significantly enhancing model performance. The model combining VIs, TFs, and PTs achieved the highest accuracy, with R^2 values of 0.794, 0.741, and 0.737 for PLSR, LASSO, and RF, respectively, outperforming the VIs + TFs model by 0.051, 0.014, and 0.023. These results demonstrate the potential of PTs to improve disease detection accuracy as fusion features. The synergistic effect of cross-dimensional features enables the model to capture more comprehensive information on powdery mildew.

4.3. Challenges and Prospects

This study developed a rubber tree powdery mildew monitoring model by combining spatial-spectral features and plant traits. Despite achieving promising results, with the best model reaching an R^2 of 0.794, there are still some limitations. Firstly, the dataset was constructed from 55 sample points collected from Ganlanba and Dongfeng farms. Although it covers multiple sites, the geographic range remains limited, so model generalizability across different temporal and spatial scales needs further validation. Future research will systematically expand the sampling to broader regions, collect multi-year and multi-phenological stage data, and integrate external datasets for independent validation, thereby enhancing the model's scalability and robustness under diverse temporal and spatial conditions. It was also assumed that sampling 50 representative leaflets per plot would adequately capture plot-scale disease severity. While this is a common practice in plant pathology, it may still underestimate within-plot heterogeneity, particularly under complex canopy conditions. In addition, although the SPAD-502 handheld chlorophyll meter was carefully cleaned before each measurement, repeated field use may have introduced a slight bias due to residual leaf material or frequent handling. Moreover, spatial resolution has increasingly attracted attention in remote sensing studies, as pixel information varies with resolution. Selecting the appropriate spatial resolution can enhance monitoring efficiency (Dash et al., 2017). This study only considered the original image resolution; future research will explore the impact of resolution on monitoring accuracy to identify the optimal resolution for rubber tree powdery mildew monitoring.

In recent years, the continuous updating of high spatiotemporal resolution satellite data has made large-scale, high-precision disease monitoring possible. UAVs are particularly well suited for fine-scale, high-frequency monitoring at the plantation level, while satellites can complement them by providing broader spatial coverage, temporal continuity, and long-term monitoring at regional to global scales. The occurrence of rubber tree powdery mildew is closely related to factors

such as phenological stages, climate conditions, and pathogen density (Liyanage et al., 2016), and remote sensing technology offers advantages in obtaining host status and habitat information. Therefore, future research will explore integrating UAV-based features with habitat-related information for rubber trees and extend the monitoring framework to satellite platforms, while also placing greater emphasis on enhancing its interpretability and operational feasibility, thereby providing valuable decision support for plantation management.

5. Conclusions

This study fully leveraged the detailed information contained in UAV hyperspectral images and proposed a rubber tree powdery mildew monitoring model that combines spatial-spectral features and plant traits. This is the first attempt in the research community to invert PTs at the canopy scale for monitoring rubber tree powdery mildew. The results demonstrated that key PTs inverted from UAV hyperspectral data can effectively characterize the severity of powdery mildew infection in rubber trees. Compared with models built on single feature types, the incorporation of PTs significantly improved model performance. The multiple feature model integrating VIs, TFs, and PTs achieved the best performance, with an R^2 of 0.794 and an RMSE of 7.991. This advantage stems mainly from the model's ability to capture subtle spectral and spatial variations induced by infection and the associated physiological and biochemical responses, providing a more robust technical pathway for disease monitoring. The successful inversion of rubber tree canopy-scale PTs also provides valuable practical experience for extending leaf-level biochemical information to broader spatial scales, laying a solid foundation for large-scale and precise monitoring in the future. Future research will further expand the spatiotemporal coverage of field data and explore the integration of multi-source satellite remote sensing to develop a cross-scale disease feature characterization framework, providing strong support for efficient monitoring and precise control of rubber tree powdery mildew at the regional scale.

CRediT authorship contribution statement

Xiangzhe Cheng: Writing – review & editing, Writing – original draft, Visualization, Validation, Methodology, Investigation, Formal analysis, Data curation, Conceptualization. **Wenjiang Huang:** Writing – review & editing, Supervision, Project administration, Investigation, Funding acquisition. **Anting Guo:** Writing – review & editing, Software, Methodology, Investigation, Conceptualization. **Zhiying Cai:** Resources, Project administration, Investigation, Funding acquisition. **Yingying Dong:** Supervision, Software. **Bohai Hu:** Investigation, Data curation. **Guiliang Chen:** Resources, Investigation, Data curation. **Haipeng Su:** Resources, Investigation. **Lanlan Li:** Resources, Investigation.

Declaration of competing interest

The authors declare that they have no known competing financial interests or personal relationships that could have appeared to influence the work reported in this paper.

Acknowledgments

This article was supported by the Science and Technology Talent and Platform Project (202405AF140032), Sino–UK Crop Pest and Disease Forecasting & Management Joint Laboratory (183611ZYLH20240009), Research on Remote Sensing Monitoring of Crop Growth and Disease and Pest under the Background of Climate Change (E44702010T), the National Natural Science Foundation of China (42201365), Hainan Provincial Natural Science Foundation of China (422QN349).

Appendix A. Supplementary material

Supplementary data to this article can be found online at https://doi.org/10.1016/j.compag.2025.111274.

Data availability

Data will be made available on request.

References

Abdulridha, J., Ampatzidis, Y., Roberts, P., Kakarla, S.C., 2020. Detecting powdery mildew disease in squash at different stages using UAV-based hyperspectral imaging and artificial intelligence. Biosystems Eng. 197, 135–148.
Alasalvar, C., Grigor, J.M., Zhang, D., Quantick, P.C., Shahidi, F., 2001. Comparison of volatiles, phenolics, sugars, antioxidant vitamins, and sensory quality of different colored carrot varieties. J. Agric. Food Chem. 49, 1410–1416.
Ashourloo, D., Mobasheri, M.R., Huete, A., 2014. Developing two spectral disease indices for detection of wheat leaf rust (Pucciniatriticina). Remote Sens. (Basel) 6, 4723–4740.
Baraldi, A., Panniggiani, F., 1995. An investigation of the textural characteristics associated with gray level cooccurrence matrix statistical parameters. IEEE Trans. Geosci. Remote Sens. 33, 293–304.
Bhandari, M., Ibrahim, A.M.H., Xue, Q., Jung, J., Chang, A., Rudd, J.C., Maeda, M., Rajan, N., Neely, H., Landivar, J., 2020. Assessing winter wheat foliage disease severity using aerial imagery acquired from small Unmanned Aerial Vehicle (UAV). Comput. Electron. Agric. 176, 105665.
Bravo, C., Moshou, D., West, J., McCartney, A., Ramon, H., 2003. Early disease detection in wheat fields using spectral reflectance. Biosyst. Eng. 84, 137–145.
Breiman, L., 2001. Random forests. Mach. Learn. 45, 5–32.
Caicedo, J.P.R., Verrelst, J., Muñoz-Marí, J., Moreno, J., Camps-Valls, G., 2014. Toward a semiautomatic machine learning retrieval of biophysical parameters. IEEE J. Sel. Top. Appl. Earth Obs. Remote Sens. 7, 1249–1259.
Calderón, R., Navas-Cortés, J.A., Lucena, C., Zarco-Tejada, P.J., 2013. High-resolution airborne hyperspectral and thermal imagery for early detection of *Verticillium* wilt of olive using fluorescence, temperature and narrow-band spectral indices. Remote Sens. Environ. 139, 231–245.
Camino, C., Calderón, R., Parnell, S., Dierkes, H., Chemin, Y., Román-Écija, M., Montes-Borrego, M., Landa, B.B., Navas-Cortes, J.A., Zarco-Tejada, P.J., Beck, P.S.A., 2021. Detection of Xylella fastidiosa in almond orchards by synergic use of an epidemic spread model and remotely sensed plant traits. Remote Sens. Environ. 260, 112420.
Cheng, X., Feng, Y., Guo, A., Huang, W., Cai, Z., Dong, Y., Guo, J., Qian, B., Hao, Z., Chen, G., Liu, Y., 2024a. Detection of rubber tree powdery mildew from leaf level hyperspectral data using continuous wavelet transform and machine learning. Remote Sens. (Basel) 16, 105.
Cheng, X., Huang, M., Guo, A., Huang, W., Cai, Z., Dong, Y., Guo, J., Hao, Z., Huang, Y., Ren, K., Hu, B., Chen, G., Su, H., Li, L., Liu, Y., 2024b. Early detection of rubber tree powdery mildew by combining spectral and physicochemical parameter features. Remote Sens. (Basel) 16, 1634.
Dash, J.P., Watt, M.S., Pearse, G.D., Heaphy, M., Dungey, H.S., 2017. Assessing very high resolution UAV imagery for monitoring forest health during a simulated disease outbreak. ISPRS J. Photogramm. Remote Sens. 131, 1–14.
Deng, X., Zhu, Z., Yang, J., Zheng, Z., Huang, Z., Yin, X., Wei, S., Lan, Y., 2020. Detection of citrus huanglongbing based on multi-input neural network model of UAV hyperspectral remote sensing. Remote Sens. (Basel) 12, 2678.
Ecke, S., Dempewolf, J., Frey, J., Schwaller, A., Endres, E., Klemmt, H.-J., Tiede, D., Seifert, T., 2022. UAV-based forest health monitoring: a systematic review. Remote Sens. (Basel) 14, 3205.
FAO, 2024. The state of the world's forests 2024. FAO.
Guo, A., Huang, W., Dong, Y., Ye, H., Ma, H., Liu, B., Wu, W., Ren, Y., Ruan, C., Geng, Y., 2021. Wheat yellow rust detection using UAV-based hyperspectral technology. Remote Sens. (Basel) 13, 123.
Guo, A., Huang, W., Ye, H., Dong, Y., Ma, H., Ren, Y., Ruan, C., 2020. Identification of wheat yellow rust using spectral and texture features of hyperspectral images. Remote Sens. (Basel) 12, 1419.
Haboudane, D., Miller, J.R., Tremblay, N., Zarco-Tejada, P.J., Dextraze, L., 2002. Integrated narrow-band vegetation indices for prediction of crop chlorophyll content for application to precision agriculture. Remote Sens. Environ. 81, 416–426.
Haralick, R.M., Shanmugam, K., Dinstein, I., 1973. Textural Features for Image Classification. IEEE Transactions on Systems, Man, and Cybernetics SMC-3, 610–621.
Hornero, A., Hernández-Clemente, R., North, P.R.J., Beck, P.S.A., Boscia, D., Navas-Cortes, J.A., Zarco-Tejada, P.J., 2020. Monitoring the incidence of *Xylella fastidiosa* infection in olive orchards using ground-based evaluations, airborne imaging spectroscopy and Sentinel-2 time series through 3-D radiative transfer modelling. Remote Sens. Environ. 236, 111480.
Huang, L., Wu, Z., Huang, W., Ma, H., Zhao, J., 2019. Identification of fusarium head blight in winter wheat ears based on fisher's linear discriminant analysis and a support vector machine. Appl. Sci. 9, 3894.
Huang, W., Lamb, D.W., Niu, Z., Zhang, Y., Liu, L., Wang, J., 2007. Identification of yellow rust in wheat using in-situ spectral reflectance measurements and airborne hyperspectral imaging. Precis. Agric. 8, 187–197.

Jacquemoud, S., Verhoef, W., Baret, F., Bacour, C., Zarco-Tejada, P.J., Asner, G.P., François, C., Ustin, S.L., 2009. PROSPECT + SAIL models: a review of use for vegetation characterization. Remote Sens. Environ., Imaging Spectrosc. Special Issue 113, S56–S66.

Jiang, X., Zhen, J., Miao, J., Zhao, D., Wang, J., Jia, S., 2021. Assessing mangrove leaf traits under different pest and disease severity with hyperspectral imaging spectroscopy. Ecol. Ind. 129, 107901.

Limkaisang, S., Kom-un, S., Takamatsu, S., Furtado, E.L., Liew, K.W., Salleh, B., Sato, Y., 2005. Molecular phylogenetic and morphological analyses of Oidium heveae, a powdery mildew of rubber tree. Mycoscience 46, 220–226.

Liyanage, K.K., Khan, S., Mortimer, P.E., Hyde, K.D., Xu, J., Brooks, S., Ming, Z., 2016. Powdery mildew disease of rubber tree. For. Pathol. 46, 90–103.

Liyanage, S., Jacob, C.K., 1992. Diseases of economic importance in rubber. In: Developments in Crop Science. Elsevier, pp. 324–359.

Maimaitijiang, M., Sagan, V., Sidike, P., Maimaitiyiming, M., Hartling, S., Peterson, K.T., Maw, M.J., Shakoor, N., Mockler, T., Fritschi, F.B., 2019. Vegetation index weighted canopy volume model (CVMVI) for soybean biomass estimation from unmanned aerial system-based RGB imagery. ISPRS J. Photogramm. Remote Sens. 151, 27–41.

Martins, G.D., Galo, M.D.L.B.T., Vieira, B.S., 2017. Detecting and mapping Root-Knot Nematode infection in coffee crop using remote sensing measurements. IEEE J. Sel. Top. Appl. Earth Observations Remote Sens. 10, 5395–5403.

Merton, R., 1998. Monitoring community hysteresis using spectral shift analysis and the red-edge vegetation stress index. In: Proceedings of the Seventh Annual JPL Airborne Earth Science Workshop. JPL Pasadena, CA, USA, pp. 12–16.

Moshou, D., Bravo, C., Oberti, R., West, J., Bodria, L., McCartney, A., Ramon, H., 2005. Plant disease detection based on data fusion of hyper-spectral and multi-spectral fluorescence imaging using Kohonen maps. Real-Time Imaging, Spectral Imaging II 11, 75–83.

Oerke, E.-C., Herzog, K., Toepfer, R., 2016. Hyperspectral phenotyping of the reaction of grapevine genotypes to Plasmopara viticola. J. Exp. Bot. 67, 5529–5543.

Poblete, T., Camino, C., Beck, P.S.A., Hornero, A., Kattenborn, T., Saponari, M., Boscia, D., Navas-Cortes, J.A., Zarco-Tejada, P.J., 2020. Detection of *Xylella fastidiosa* infection symptoms with airborne multispectral and thermal imagery: Assessing bandset reduction performance from hyperspectral analysis. ISPRS J. Photogramm. Remote Sens. 162, 27–40.

Poblete, T., Navas-Cortes, J.A., Camino, C., Calderon, R., Hornero, A., Gonzalez-Dugo, V., Landa, B.B., Zarco-Tejada, P.J., 2021. Discriminating *Xylella fastidiosa* from *Verticillium dahliae* infections in olive trees using thermal- and hyperspectral-based plant traits. ISPRS J. Photogramm. Remote Sens. 179, 133–144.

Richardson, A.D., Duigan, S.P., Berlyn, G.P., 2002. An evaluation of noninvasive methods to estimate foliar chlorophyll content. New Phytol. 153, 185–194.

Robnik-Šikonja, M., Kononenko, I., 2003. Theoretical and empirical analysis of ReliefF and RReliefF. Mach. Learn. 53, 23–69.

Su, J., Liu, C., Coombes, M., Hu, X., Wang, C., Xu, X., Li, Q., Guo, L., Chen, W.-H., 2018. Wheat yellow rust monitoring by learning from multispectral UAV aerial imagery. Comput. Electron. Agric. 155, 157–166.

Tagliabue, G., Boschetti, M., Bramati, G., Candiani, G., Colombo, R., Nutini, F., Pompilio, L., Rivera-Caicedo, J.P., Rossi, M., Rossini, M., 2022. Hybrid retrieval of crop traits from multi-temporal PRISMA hyperspectral imagery. ISPRS J. Photogramm. Remote Sens. 187, 362–377.

Tibshirani, R., 1996. Regression shrinkage and selection via the lasso. J. R. Stat. Soc. Ser. B Stat Methodol. 58, 267–288.

Torriani, S.F.F., Melichar, J.P.E., Mills, C., Pain, N., Sierotzki, H., Courbot, M., 2015. Zymoseptoria tritici: a major threat to wheat production, integrated approaches to control. Fungal Genet. Biol.Septoria Tritici Blotch Disease of Wheat: Tools and Techniques to Study the Pathogen Zymoseptoria Tritici 79, 8–12.

Van Beilen, J.B., Poirier, Y., 2007. Establishment of new crops for the production of natural rubber. Trends Biotechnol. 25, 522–529.

Verrelst, J., Camps-Valls, G., Muñoz-Marí, J., Rivera, J.P., Veroustraete, F., Clevers, J.G. P.W., Moreno, J., 2015. Optical remote sensing and the retrieval of terrestrial vegetation bio-geophysical properties – a review. ISPRS J. Photogramm. Remote Sens. 108, 273–290.

Verrelst, J., Romijn, E., Kooistra, L., 2012. Mapping vegetation density in a heterogeneous river floodplain ecosystem using pointable CHRIS/PROBA data. Remote Sens. (Basel) 4, 2866–2889.

Wang, L., 2014. Physiological and molecular responses to drought stress in rubber tree (Hevea brasiliensis Muell. Arg.). Plant Physiol. Biochem. 83, 243–249.

Wold, S., Sjöström, M., Eriksson, L., 2001. PLS-regression: a basic tool of chemometrics. Chemom. Intel. Lab. Syst. 58, 109–130.

Wu, Y., Zhao, Q., Yin, X., Wang, Y., Tian, W., 2023. Multi-parameter health assessment of jujube trees based on unmanned aerial vehicle hyperspectral remote sensing. Agric.-London 13, 1679.

Xu, L., Shi, S., Gong, W., Shi, Z., Qu, F., Tang, X., Chen, B., Sun, J., 2022. Improving leaf chlorophyll content estimation through constrained PROSAIL model from airborne hyperspectral and LiDAR data. Int. J. Appl. Earth Obs. Geoinf. 115, 103128.

Zarco-Tejada, P.J., Camino, C., Beck, P.S.A., Calderon, R., Hornero, A., Hernández-Clemente, R., Kattenborn, T., Montes-Borrego, M., Susca, L., Morelli, M., Gonzalez-Dugo, V., North, P.R.J., Landa, B.B., Boscia, D., Saponari, M., Navas-Cortes, J.A., 2018. Previsual symptoms of Xylella fastidiosa infection revealed in spectral plant-trait alterations. Nat. Plants 4, 432–439.

Zeng, T., Zhang, H., Li, Y., Yin, C., Liang, Q., Fang, J., Fu, W., Wang, J., Zhang, X., 2023. Monitoring the severity of rubber tree infected with powdery mildew based on UAV multispectral remote sensing. Forests 14, 717.

Zhang, H., Huang, L., Huang, W., Dong, Y., Weng, S., Zhao, J., Ma, H., Liu, L., 2022. Detection of wheat Fusarium head blight using UAV-based spectral and image feature fusion. Front. Plant Sci. 13, 1004427.

Zhang, J., Huang, Y., Pu, R., Gonzalez-Moreno, P., Yuan, L., Wu, K., Huang, W., 2019. Monitoring plant diseases and pests through remote sensing technology: a review. Comput. Electron. Agric. 165, 104943.

Zhang, J., Lin, Y., Wang, J., Huang, W., Chen, L., Zhang, D., 2012a. Spectroscopic leaf level detection of powdery mildew for winter wheat using continuous wavelet analysis. J. Integr. Agric. 11, 1474–1484.

Zhang, J., Pu, R., Wang, J., Huang, W., Yuan, L., Luo, J., 2012b. Detecting powdery mildew of winter wheat using leaf level hyperspectral measurements. Comput. Electron. Agric. 85, 13–23.

Zhang, J., Qiu, X., Wu, Y., Zhu, Y., Cao, Q., Liu, X., Cao, W., 2021. Combining texture, color, and vegetation indices from fixed-wing UAS imagery to estimate wheat growth parameters using multivariate regression methods. Comput. Electron. Agric. 185, 106138.

Zhao, Y.-R., Li, X., Yu, K.-Q., Cheng, F., He, Y., 2016. Hyperspectral Imaging for determining pigment contents in cucumber leaves in response to angular leaf spot disease. Sci. Rep. 6, 27790.

Zheng, H., Cheng, T., Zhou, M., Li, D., Yao, X., Tian, Y., Cao, W., Zhu, Y., 2019. Improved estimation of rice aboveground biomass combining textural and spectral analysis of UAV imagery. Precis. Agric. 20, 611–629.